LUND UNIVERSITY
Faculty of Science

Feasibility of new Dark Matter search at ATLAS

Peter Stratmann

Thesis submitted for the degree of Bachelor of Science
Project duration: 2 months

Supervised by C.W. Kalderon and C. Doglioni

Department of Physics
Division of Particle Physics
May 2017

LUND UNIVERSITY

Abstract

Particle Physics

Bachelor's Thesis

Feasibility of new Dark Matter search at ATLAS

This thesis examines the idea of calibrating Level 1 jets. These are used in the Trigger-Level Analysis at the ATLAS in the search for a new mediator, in this case between Standard Model and Dark Matter particles. In the thesis, the idea to calibrate the Level 1 jets is investigated. To calibrate the Level 1 jets, they are divided into bins of transverse momentum and pseudorapidity. The responses are then taken to calibrate the transverse momenta of the Level 1 jets, in order to shift the invariant dijet mass towards the real value, and to improve the resolution of its distribution. It is shown that the calibration does not only shift the value, but indeed improves the resolution to a certain extent. To further improve the resolution, a finer binning and taking detector effects into consideration is suggested. The calibration of the Level 1 jets is used to examine in how far a new search for Dark Matter using these jets is feasible.

Popular Science

Looking into the night sky has always fascinated mankind. All who have observed the stars have asked themselves what is out there. Better and better telescopes have enabled us to take an ever deeper look into the universe, and with it a look into the past. Now we know that what we can see, however, only accounts for a small percentage of what is out there. Only about 15% of the total matter in the universe is ordinary matter as we know it and of which we ourselves are made. The rest is called Dark Matter, and even though we know it must be there, we actually have no idea what it is. The term "dark" is somewhat misleading, as Dark Matter is not dark, but invisible, as it does not interact electromagnetically.

But how do we know that it is there when we cannot see it? We mainly know of its existence because it interacts with ordinary matter through gravity. One of the first pieces of evidence came from the Swiss astronomer Fritz Zwicky. In 1933, he measured how fast different galaxy clusters, that is a group of gravitationally bound galaxies, rotate and figured out that they rotate so fast that the galaxies should not keep together. Like on a playground roundabout that is spinning too fast, they should drift apart. There must be something that keeps them together, namely Dark Matter. Over time, many other pieces of evidence have been added that all speak in favour of Dark Matter.

The problem is, we know it is there, but we do not know what it is. All particles - so the most elementary building blocks everything is made of - that are known to us are summed up in the *Standard Model of Particle Physics*. It consists of *fermions* and *bosons*. Fermions are the particles all matter known to us (so you, too) is made of. Fermions can interact with each other through forces. One force most people will know is the electromagnetic force, it is the one that makes your hair all fuzzy when you rub a balloon against it. There are four known elementary forces, three of which are mediated through bosons. One can imagine it this way: one particle gives away a boson, the other particle takes it in, and in doing so they feel a force between them.

Scientists are looking for Dark Matter in the ATLAS experiment at CERN in Switzerland, the largest laboratory of its kind in the world. In ATLAS, protons - which, together with neutrons, make up atoms' cores - are shot together at very high energies to create new particles, for example Dark Matter particles. This may be odd for people who are not familiar with it; after all it is as if two ducks crash and come out as cars. This can, however, not happen directly but needs a boson (we talked about these before) to do

so. Actually, we must look deeper. A proton is a bag of quarks (this is what they are made of). When two of these quarks collide, they can form a boson together, and the boson splits up into two Dark Matter particles. The Dark Matter particles can not be seen or otherwise detected, so what should we do? We are lucky: if two quarks can make a boson, the boson can not only make Dark Matter particles, but can also split up back into two quarks. When this happens, the quarks are so fast that they can create many more particles and we get two cones of particles. These cones - they are called jets - can then be detected and from their properties, the mass of the boson can be deduced. The hope is to find a new, yet unknown boson which can give a hint to Dark Matter. This search is like hunting for an invisible deer by searching for its footprints in the snow.
But there is a problem: every second, thousands of millions protons collide. Everyone can imagine that this creates a huge amount of data. If all these data would be saved on CDs, the stack of CDs needed every year would reach twice to the moon and back again. It is obvious that some kind of trigger is needed that tells us if an event (that is what it is called when a collision takes place) is interesting to look at or not. My thesis is looks at a new way how this can be done and in how far it has advantages to how it is done currently. If it is successful, it might also help to examine events that would otherwise be lost, even though they might be interesting.

Acknowledgements

Special thanks go to my supervisor Will Kalderon and my co-supervisor Caterina Doglioni. They always took the time to guide me through this project and explain everything that needed explanation.
I also want to thank the whole division of Particle Physics for the friendly atmosphere I could always find.

Contents

Abbreviations & Symbols

ATLAS	A Toroidal LHC ApparatuS
CERN	European Organization for Nuclear Research
CMB	Cosmic Microwave Background
ΔR	Angular separation
ECAL	Electromagnetic Calorimeter
η	Pseudorapidity
HCAL	Hadronic Calorimeter
HLT	High Level Trigger
LHC	Large Hadron Collider
L1	Level 1
MACHO	Massive Compact Halo Object
m_{jj}	Dijet invariant mass
Njets	Number of jets
RoI	Region of Interest
ϕ	Azimuthal angle
p_T	Transverse momentum
TLA	Trigger-Level Analysis
WIMP	Weakly Interacting Massive Particle

Chapter 1

Introduction

Dark Matter is one of the big mysteries of modern cosmology. Its existence is commonly assumed, but not much is known about its properties [1]. Apart from trying to detect Dark Matter that already exists, research involves attempts to produce it in particle colliders. One approach in the search for Dark Matter, that is among several performed at the ATLAS experiment, is to look for the presence of a mediator particle between Dark Matter and quarks, which is necessary in many simplified models in order for Dark Matter to be directly produced at the LHC. Because the mediator would have to couple to quarks as well as the Dark Matter particles, it can also decay back into quarks. The quarks would subsequently hadronise and produce two highly energetic jets. Therefore, one class of Dark Matter searches is for dijet resonances corresponding to such a mediator [2].

The huge number of collisions in the collider results in an enormous data rate, that is the number of events times the event size. This amount of data cannot be read off the detector or stored. In order to keep the data rate within a feasible limit, either the event size or the event rate has to be reduced. The trigger system reduces the event rate by identifying events with jets above a certain energy threshold, since these are typically the most interesting events, but this causes a loss in information and hence sensitivity to lower mass resonances. A Trigger-Level Analysis partially overcomes this problem through recording smaller events (only with objects available to the trigger system) with less detailed information, allowing a higher event rate to be recorded and recovering sensitivity to lower mass resonances [3].

In this thesis, a new idea for a search involving the use of L1 jets - jets at the first level of the Trigger-Level Analysis - is examined. The use of these objects may allow a higher

event rate and give the opportunity to record more interesting events for low-mass dijet resonances. For this new search to be successful, L1 jets must be calibrated. It is studied how a calibration of the L1 jets' transverse momenta - where the calibration is dependent on the L1 jets' transverse momenta and pseudorapidities - can achieve this.
The thesis first gives a summary of the necessary background information. Firstly, Dark Matter is explained. Evidence for its existence and particles that could come into consideration for Dark Matter particles are given and the detection of Dark Matter particles is described. Secondly, two-particle collisions and their kinematics are introduced, and dijet events are described shortly. Thirdly, the ATLAS Detector, its functionality, and its use to detect Dark Matter particles is presented; furthermore, the idea behind the Trigger-Level Analysis is shown.
The second part shows the studies that are conducted. First, a look is taken at a simulation of a mediator decaying to quarks at truth level. This is done to get a first impression of the characteristics of a signal and how the kinematics of a dijet event behave like. Second, a simulation of another mediator decaying to quarks is studied. This time, however, the kinematics are compared at truth level as well as at different levels of the Trigger-Level Analysis. Based on these, a calibration of the L1 jets is performed. The transverse momenta of the L1 jets are calibrated, according to the transverse momentum and pseudorapidity the respective jet has. Lastly, the transverse momentum and dijet invariant mass distributions of the so calibrated jets are compared to the uncalibrated jets as well as to the trigger jets - jets used in the Trigger-Level Analysis.

Chapter 2

Search for Dark Matter

2.1 Dark Matter

2.1.1 Evidence

Several early observations indicated that there must me more mass in galaxies than only the luminous mass. In the 1970s, Vera Rubin, together with other physicists, studied galactic rotational curves and found that the rotational velocities of the studied galaxies stayed constant near the edges. However, with the assumed mass distribution - that most of the mass is located in the galaxy's centre, - velocity should decrease at the edges of the galaxies. A possible explanation was the existence of further mass that is not visible, the so called Dark Matter [1].

A first assumption was that Dark Matter consists of ordinary baryonic matter, namely so called MACHOs (Massive compact halo objects). These MACHOs include, among others, planets, black holes, and neutron stars. To examine this possibility, researchers searched for cases of gravitational microlensing. Gravitational microlensing, as first stated in Einstein's theory of general relativity, changes the brightness of distant cosmic objects due to the gravity of closer objects. The low number of such cases found indicates that the Dark Matter distribution is diffuse rather than compact, so that MACHOs can only account for a small part of Dark Matter [1].
There are other indications that contradict a high amount of Dark Matter made up by (even diffuse) baryonic matter. One indication comes from the Cosmic Microwave

Background (CMB), which was created 380,000 years after Big Bang. The CMB is remarkably isomorph, but has anisotropies [4]. Studying the power spectrum, that is, the temperature fluctuations of the CMB against different angular scales, provides information about the composition of the early universe. With it, the amount of total matter and baryonic matter can be determined. Indeed, baryonic matter only makes up a small part of the total matter [5].

All these points taken together indicate the existence of Dark Matter, while disfavouring other explanatory approaches, like modified gravity, for example.

2.1.2 Possible Particles

All particles that are known today and the all interactions between them apart from gravity are described in the Standard Model of particle physics. The Standard Model only consists of a small number of particles. The particles are grouped in three categories: the spin-$\frac{1}{2}$ fermions, the spin-1 gauge bosons, and the spin-0 Higgs-boson. The fermions contain the quarks and leptons; the gauge bosons are the mediators of the three elemental forces; the Higgs-boson explains why the other particles in the Standard Model have mass. It is assumed that all particles in the Standard Model are elementary, that is, they have no further substructure [6].
The Standard Model is very successful in describing and explaining phenomena in particle physics. However, it does not offer a plausible candidate for Dark Matter particles. Neutrinos, though being stable and only weakly interacting, can not account for the whole amount of Dark Matter. In a universe where neutrinos dominated the amount of mass, larger structures would have arranged first. Observations and simulations show that this is not likely, though [1].

Possible candidates for Weakly Interacting Massive Particles (WIMPs) - particles that may constitute Dark Matter - can be found in Supersymmetry (SUSY). SUSY assigns to every fermion in the Standard Model a boson superpartner and to every boson a fermion superpartner. Every particle has the same properties as its superpartner, save the spin. Due to symmetry breaking however, the superpartners mostly have much higher masses than the respective particles. SUSY might offer several neutral candidates that interact weakly and could act as Dark Matter. A first candidate is the sneutrino, the superpartner of the neutrino. These, however, would have been annihilated very

quickly in the early universe. A second candidate is the gravitino, the superpartner of the graviton, a possible mediator of the gravitational force. Gravitinos could only act as hot Dark Matter, though, and it is known that most Dark Matter must be cold to be consistent with observations. This leaves a third candidate, the neutralino, which is a neutral superposition of the Higgs and gauge bosons superpartners. In most versions of SUSY, the neutralino is the lightest supersymmetric partner. In the case where R-parity - where all Standard Model particles have R-parity 1 and all supersymmetric particles -1 - is conserved, this would mean that as the lightest supersymmetric particle can not decay and the neutralino would be stable. Hence, neutralinos are an excellent candidate for Dark Matter [1].

Further candidates are considered for Dark Matter. These include the axion, a particle proposed by Robert Peccei and Helen Quinn, or its superpartner, the axino. Other candidates may come from theories of extra spatial dimensions, as proposed for example by Theodor Kaluza and Oscar Klein [1].

2.1.3 Detection

One possible way to detect Dark Matter particles is to detect them directly. The basic idea behind this is to use a detector with a large amount of one element, in order to increase the probability of an interaction. It has to be ensured that no radioactive contamination is present and that it is shielded against background. Furthermore, the detector should be operational for a long time to increase the number of possible events [1].
A signal caused by a WIMP can be recognised by its characteristics. Firstly, as WIMPs are ubiquitous, the signal should have an even distribution throughout the detector. Secondly, the event should be single-site. Thirdly, as the energy the WIMP leaves in the detector depends on its velocity, the detection rate should change during the course of a year, dependent on the movement of earth relative to the Dark Matter in the galaxy [1]. Interactions of the Dark Matter particle with the detector material can be distinguished. The interaction can be elastic or inelastic, and spin-dependent or spin-independent. With elastic scattering, the nucleus as a whole recoils. This can be detected thermally, giving a vibration in the crystal lattice of the detector, through scintillation, where a bound electron is excited to an higher energy state and then deexcites through photon emission,

or through ionisation, where the energy deposited is large enough to free a bound electron. In the case of inelastic scattering, the nucleus is excited to a higher energy state and later deexcites emitting a photon. Furthermore, an event can be characterised if it spin-dependent, that is, if the spin of the WIMP couples to the spin of the nucleus with which it interacts [1].

Another way to look for Dark Matter is to detect it indirectly. This takes advantage of the fact that, in SUSY, neutralinos are their own antiparticles, so that they can annihilate with themselves. They can create two photons in the range of gamma-radiation. It is believed to happen mostly in the galactic centre. Further products resulting from annihilation are neutrinos and antimatter [1].

2.2 Two-particle Collisions

2.2.1 Dijets

According to Quantum Chromodynamics, particles that are interacting strongly, that is, quarks and gluons, have a further quantum number, called colour. Particles with colour cannot appear freely, but only in colourless combinations with other particles. If quarks or antiquarks are separated from each other, the field lines of the colour field stay in a colour string. The force stays constant while the energy increases. For high energies, the string may break - primarily at its ends, - creating quark-antiquark pairs. The quarks then build hadrons, which is called hadronisation. This means that hadrons are created close to the original quarks, moving in a similar direction. This can repeat itself, giving cones with many hadrons, so called jets. In highly energetic events in which two quarks are created, this results in two jets. These events are called dijet events [7].

2.2.2 Kinematics

In this thesis, as it is normally done in High-energy physics, the natural units $c = \hbar = 1$ are used. Since collisions occur at high velocities, the four-vector notation is useful. The covariant four-momentum is then given in eq. 2.1 as

$$p^\mu = \left(p^0, p^1, p^2, p^3\right) = (E, \vec{p}) = (E, \vec{p}_T, p_z) = (E, p_x, p_y, p_z)\,, \tag{2.1}$$

where E is the energy of the particle, $\vec{p}$ the momentum, $\vec{p}_T$ the momentum transverse to the z-axis, and p_x, p_y, and p_z the momenta in direction of the x-, y-, and z-axis, respectively. The Minkowski norm of the four-momentum is then given in eq. 2.2 as

$$p^2 \equiv p \cdot p \equiv p^0 p^0 - \vec{p} \cdot \vec{p}. \tag{2.2}$$

According to the energy-momentum relation, the invariant mass of a free particle with energy E, momentum $\vec{p}$ and four-momentum p is (eq. 2.3)

$$m_0^2 = E^2 - |\vec{p}| = p^2. \tag{2.3}$$

In a two-particle collision with four-momenta p_1 and p_2, this then becomes (eq. 2.4)

$$M = (p_1 + p_2)^2 , \tag{2.4}$$

which, in the case of a dijet event, is the dijet invariant mass m_{jj}. In collisions, it is helpful to define the beam axis, that is, the axis the particles move along before the collision, as the z-axis. The transverse momentum $\vec{p}_T$ is then the momentum of the particles transverse to the beam axis. Furthermore, the azimuthal angle ϕ and the angle to the beam axis θ are then taken. With θ, the pseudorapidity η is defined in eq. 2.5 as

$$\eta = -\ln\left(\tan\frac{\theta}{2}\right). \tag{2.5}$$

η becomes 0 perpendicular to the beam line and tends towards infinity along the beam line [8]. Using the absolute value of the transverse momentum $p_T = |\vec{p}_T|$ (in the following simply called "transverse momentum"), the azimuthal angle, and the pseudorapidity, the momentum can then be calculated by eq. 2.6

$$\vec{p} = \begin{pmatrix} p_T \cos\phi \\ p_T \sin\phi \\ p_T \sinh\eta \end{pmatrix} \tag{2.6}$$

with an absolute value of $|\vec{p}| = p_T \cosh\eta$. Further properties that are used in two-particle collisions are $y^\star$, given by eq. 2.7

$$y^\star = \frac{1}{2}(\eta_1 - \eta_2), \tag{2.7}$$

with the pseudorapidities of the two particles η_1 and η_2, and the angular separations between the two particles in eq. 2.8

$$\Delta R \equiv \sqrt{(\Delta\eta)^2 + (\Delta\phi)^2}. \tag{2.8}$$

2.3 ATLAS Detector

ATLAS (A Toroidal LHC ApparatuS) is a particle physics experiment at the Large Hadron Collider (LHC) at the European Organization for Nuclear Research (CERN) in Switzerland and France. It is one of its major experiments, and is operated by an international cooperation. Its purpose is to test predictions made from the Standard Model and to look for phenomena beyond the Standard Model, for example for Dark Matter [9].

2.3.1 Particle Detection at ATLAS

The ATLAS Detector is the detector with the largest volume ever built for a particle collider. The detector's task is to measure momentum, energy, and the trajectory of the particles involved in the collision. The detector consists of four main components: the Inner Detector (ID), the Calorimeter, the Muon Spectrometer, and the Magnet System [10].

Calorimeters measure the energy of the particles through total absorption. The idea is that the particles interact with the material of the absorber, creating secondary particles that can interact again. This results in a shower of particles. There are Electromagnetic Calorimeters (EMCALs) and Hadronic Calorimeters (HCALs). The EMCAL is used to measure the energy of electrons, positrons, and photons through electromagnetic interactions. HCALs measure the energy of hadrons through strong interaction [6]. Both types of calorimeters are used in ATLAS as parts of a Liquid Argon Calorimeter, which is surrounded by a Tile Calorimeter [11]. Information about the pseudorapidity coverage, granularity and number of readout channels of the calorimeters and their components is given in ref. [12].
The ID is a tracking chamber which detects charged particles. The muon chamber is located at the edge of the experiment. Unlike many other particles, muons are not stopped by the calorimeters and so are the only particles that can give a signal in that region

[13]. The Magnet System provides a solenoidal magnetic field in the ID and a toroidal magnetic field in the muon chamber. The curvature of the particle tracks is then used to measure the momentum of the particles.

2.3.2 Dark Matter Search at ATLAS

It is known that, aside from gravitation, Dark Matter only interacts weakly if at all. In the case that there is another interaction between Dark Matter and Standard Model particles with a new mediator, however, Dark Matter particles can be produced in quark-quark collisions with this mediator. The Dark Matter particles would escape the detector undetected. However, since the mediator couples to Dark Matter and quarks, it can also decay back into two quarks, giving two jets. This event can be seen in the dijet invariant mass distribution as a bump on top of the smooth distribution at the mass of the mediator [2]. The studies conducted in this thesis are based upon the existence of this hypothetical mediator.

2.3.3 Trigger-Level Analysis

The high number of collisions in the ATLAS detector makes it impossible to store all the data. As the data rate is the number of events times the size of an event, either the event number or the event size has to be reduced. Interesting events are mainly those with high energies; for this reason, trigger systems reduce the event rate by only considering events above a certain threshold. To partially reduce the loss in information and sensitivity, a Trigger-Level Analysis (TLA), which records smaller events (only with objects available to the trigger system) with less detailed information, is used.
A first-level (L1) trigger identifies Regions of Interests (RoIs) by looking at calorimeter towers. Calorimeter towers are coarse-granularity sections of the calorimeter. The RoIs are identified with sliding-window algorithms of $\Delta\eta \times \Delta\phi = 2 \times 2$ and 4×4 groups of the towers. The L1 trigger is hardware-based. The L1 trigger passes the RoIs to the High-Level Trigger (HLT) if they meet certain criteria and are then processed. The HLT reads out more information from the calorimeters and applies calibration to the jets (trigger jets). The calorimeter cells are subsequently clustered (so called "topoclusters"). The trigger jet are then saved to disc. In the normal ATLAS analysis, a further step is applied: if the trigger jets meet certain criteria, the whole event is read out and saved to disk [3].

A new idea that is studied in this thesis is that, instead of RoIs, the L1 would identify towers above certain thresholds and pass these to the HLT.

2.4 Data Analysis

The data for this thesis come from simulations of mediators decaying to two quarks with subsequent hadronisation. The data analysis is done with PyROOT, a Python extension module with which every ROOT class can be evaluated [14]. ROOT is "[a] modular scientific software framework. It provides all the functionalities needed to deal with big data processing, statistical analysis, visualisation and storage."[15]

There are four levels in the reconstruction at ATLAS, which are further used in the studies. There is the truth level, which are the jets directly out of the simulation without any detector effects considered. Furthermore, there are the proto-jets at the first trigger level (further referred to as "L1 jets"), the trigger jets that are recorded from the HLT with limited information and further calibrated (further referred to as "HLT jets"), and the fully reconstructed and calibrated jets (further referred to as "offline jets"). For further analysis, the transverse momentum p_T, pseudorapidity η, azimuthal angle ϕ and energy E (for HLT, offline and truth jets) are used. For L1 jets, no energy is given, but the mass is set to zero, instead. The jets in the events are ordered from highest p_T to lowest p_T. The jet with the highest p_T is then called the "first leading jet" (or simply "leading jet"), the one with the second highest p_T "second leading jet" (or simply "subleading jet"), the one with the third highest p_T "third leading jet", and so on. These variables are also used to calculate the dijet invariant mass according to the energy-momentum relation (eq. 2.4).
To compare jets at different levels with each other, they are matched. This means that jets which are spatially close to each other are considered to be the same jets. The matching is important to calculate ratios, for example. The matching of two jets is done as described in the following. For a given jet at one level, the angular separation ΔR as defined in eq. 2.8 is calculated between this jet and all the jets in that event from the other level. The jets with minimal angular separation ΔR - as long as $\Delta R < 0.4$ - are then the matching jets. If ΔR is not smaller than 0.4 for any jets, no jets are matching.

Chapter 3

Results

3.1 Truth Level Kinematics

The following studies are conducted using a simulation of a mediator decaying to two quarks, which then hadronise, giving two high-energy jets. Initially, the signal kinematics are examined at truth level. The simulation is done for a mediator with a mass of $m_{\mathrm{R}} = 450\,\mathrm{GeV}$, coupling to Dark Matter particles with masses of $m_{\mathrm{DM}} = 10\,\mathrm{TeV}$. The mediator couples to quarks with a coupling constant of $g_q = 0.15$ and to Dark Matter particles with a coupling constant of $g_{\mathrm{DM}} = 1.5$.
Looking at the distribution of the transverse momentum, as seen in fig. 3.1, it is seen that the transverse momentum distributions of the leading and subleading jets a located higher than those of the subsequent jets. Most of the leading and subleading jets are the jets resulting from the hadronisation of the two quarks into which the mediator decays. The distributions slope upwards and then drop off. For the same absolute momentum, the transverse momentum increases when the jet gets closer to the transverse plane. Most of the leading jets are close to the transverse plane and thus the number of events with low transverse momenta is low. When it is in the transverse plane, the transverse momentum is maximal and equal to the absolute momentum. This explains the drop. The subsequent jets mostly derive from other effects with generally low transverse momenta, namely pile-up. Pile-up are additional proton-proton collisions which are not of interest. The pile-up consists of in-time and out-of-time pile-up, cavern background, beam halo events, and beam gas events. In-time and out-of-time pile-up are collisions during, respectively shortly before and after the actual collision of interest; the cavern background results from the gas

of photons and neutrons; beam halo events create further muons from protons scraping against a collimator; in beam gas events, protons collide with the residual gas in the beam-pipe [16].

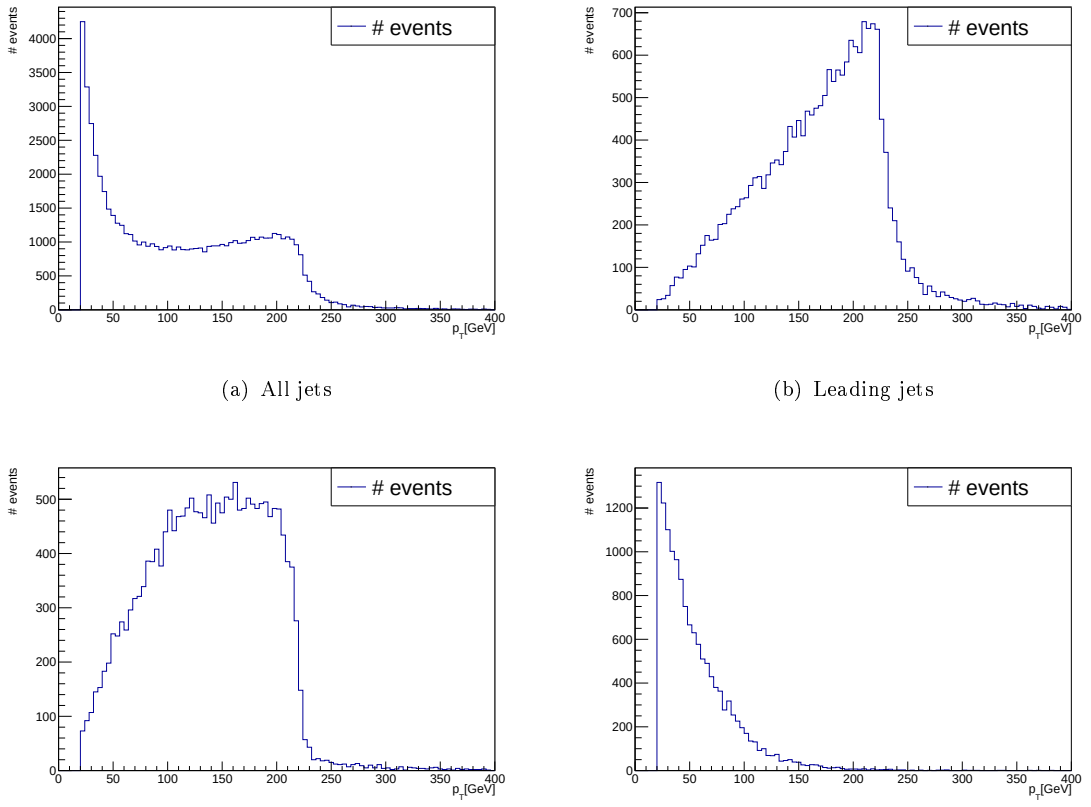

(a) All jets

(b) Leading jets

(c) Second leading jets

(d) Third leading jets

Fig. 3.1 Transverse momentum of all jets and of three leading jets.

The $y^\star$ for the leading and subleading jets are symmetric around zero. This can evidently be seen in fig. 3.2. The detector is symmetric in η. Thus, it is equally probable for the leading jet to have a higher pseudorapidity than the subleading jet than it is the other way round. In an ideal case, where the two jets are back-to-back, $y^\star$ is equal to zero. In an event with two jets, this comes from momentum conservation.

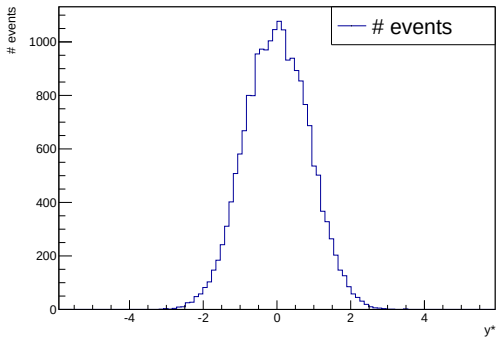

Fig. 3.2 $y^\star$ distribution for two leading jets.

The transverse momenta and $y^\star$ are used to make decisions on whether an event is considered to be interesting or not. Subsequently cuts of these are applied when calculating the invariant mass. The invariant mass distribution can be seen in fig. 3.3. It is plotted for four cases with different conditions. Firstly, all jets are taken unconditionally. Secondly, a cut of 50 GeV of the transverse momentum is applied for all leading and second leading jets. This means that only events in which the transverse momenta of the leading and subleading jet exceed this value are considered. The $p_T = 50\,\text{GeV}$ cut eliminates most of the pile-up. Thirdly, a transverse momentum cut of 220 GeV for the leading and of 85 GeV for the subleading jets is applied. Fourthly, adding to the latter condition, the absolute value of $y^\star$ between leading and subleading jets in an event must be lower than 0.6. These p_T and $y^\star$ cuts are applied by the current TLA [3].

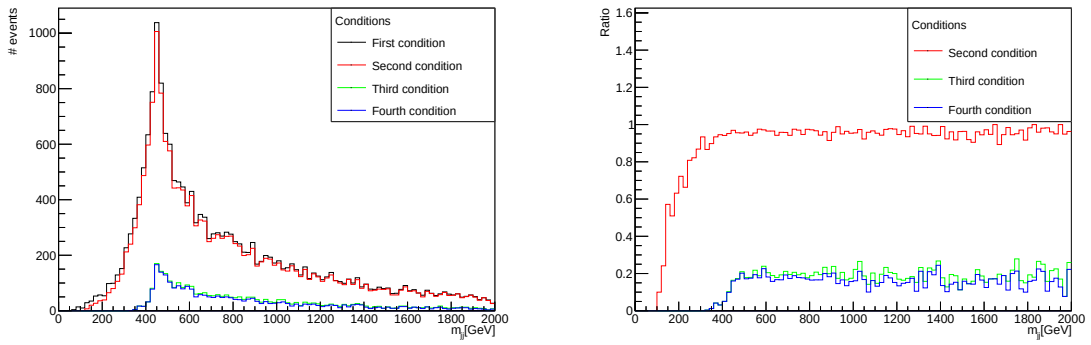

(a) Absolute values (b) Ratios

Fig. 3.3 The invariant mass distribution is plotted for the four conditions applied as previously described. In (a), the absolute number of events are plotted. In (b), the ratios of the number of events with cuts relative to the ones with no cuts applied are plotted.

It can be seen that the distributions are peaked around $m_{jj} = 450\,\text{GeV}$. The peak agrees with the mediator mass of $m_{jj} = 450\,\text{GeV}$ that is used in this simulation. The second condition, the $p_T = 50\,\text{GeV}$ cut for the leading and subleading jets, does not remove many events. Fig. 3.1 shows that only a relative low number of the leading and subleading jets have momenta lower than 50 GeV, so only few events are effected. In contrast, a large number of events is removed by the third condition. The fourth condition again does not have a large impact relative to the third. To understand the reason for this, the $y^\star$ distribution is examined for the p_T cuts applied in the third condition. This is done in fig. 3.4.

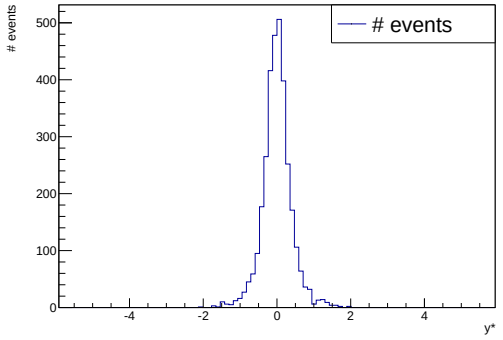

Fig. 3.4 $y^\star$ distribution for two leading jets with p_T cuts from the third condition.

In comparison to the distribution without any p_T cuts (see fig. 3.2), the $y^\star$ distribution with the p_T cuts from the third condition becomes much narrower. In fact, only a little minority of the events actually have a $y^\star$ which is higher than 0.6 in absolute values. A jet with a higher transverse momentum has a lower angular separation from the transverse plane than a jet with a lower transverse momentum, that is, if the jets have same absolute momentum. The pseudorapidity is thus lower and so is the $y^\star$, too, consequently.
From the conditions applied to the transverse momenta, it is evident that the third condition results in a large loss of events. The p_T cuts in this conditions are the ones that are applied by the current TLA. A cut at 50 GeV for both leading and subleading jets, however, preserves the majority of these events and gives a much higher peak. It is preferable to have a pronounced peak. In reality, the peak caused by the new mediator would sit on top of a smooth distribution; a broader peak would thus be harder to detect. This fact justifies the search for a new analysis in which events with lower transverse momenta can be used.

3.2 Comparison of Jet Kinematics

Having previously examined the kinematics of a simulation at truth level, the next step is to compare the kinematics at different levels of the analysis. The simulation is made for a mediator with mass $m_R = 350\,\text{GeV}$, coupling to Dark Matter particles of mass $m_{\text{DM}} = 10\,\text{TeV}$ with a coupling constant of $g_{DM} = 1.5$, and coupling to quarks with a coupling constant of $g_q = 0.1$. At first, the transverse momentum distributions for all jets together, as well as the three leading order jets separately are compared in fig. 3.5 at the different levels.

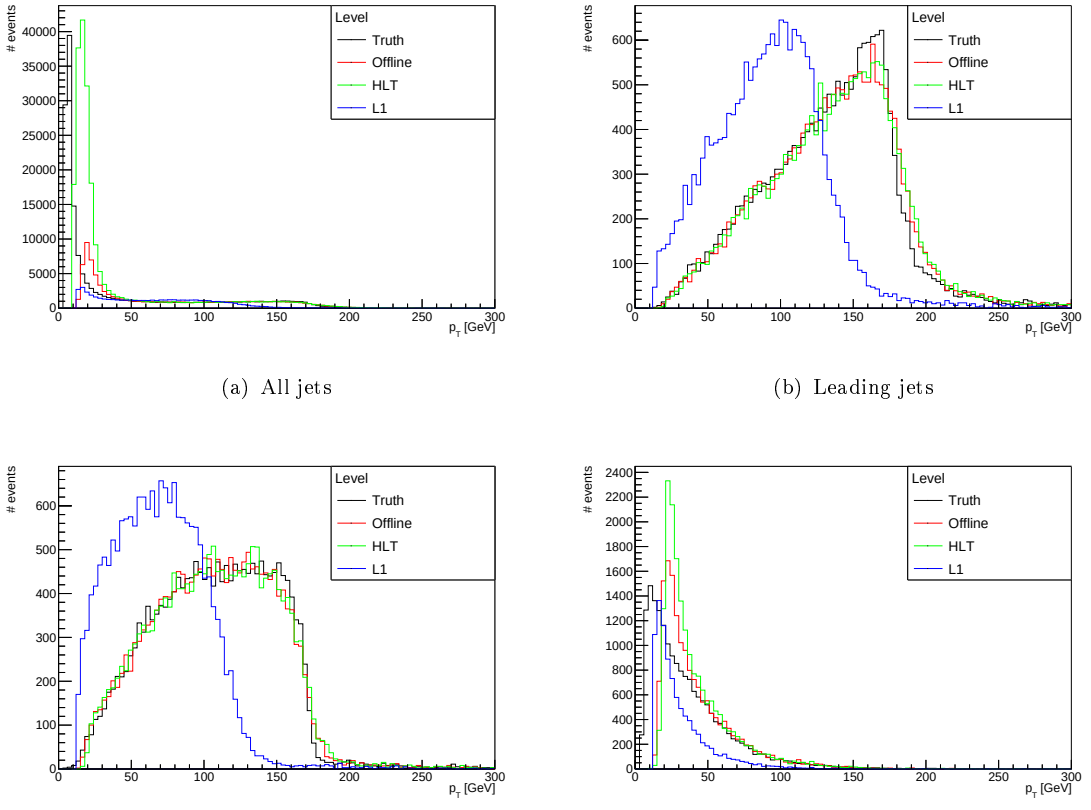

(a) All jets

(b) Leading jets

(c) Second leading jets

(d) Third leading jets

Fig. 3.5 Transverse momentum distributions for all jets combined and the three leading orders jets separately for truth, offline, HLT and L1 level.

In fig. 3.5 it seems that the L1 jets generally have lower transverse momenta than jets at other trigger levels. To verify this, it is looked at the p_T ratios compared to jets at truth level. For this, every jet at L1, HLT and offline level are matched to jets at truth

level. Fig. 3.6 shows a histogram of the ratios between the transverse momenta of all jets respective to the matching jets at truth level.

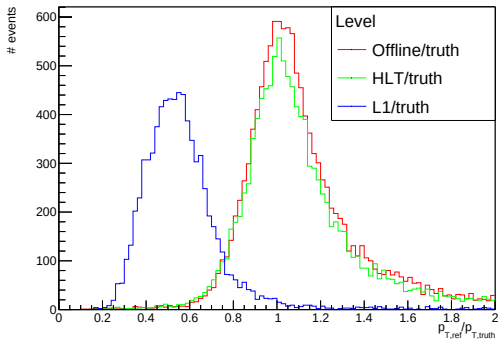

Fig. 3.6 Transverse momentum ratio of all jets combined at offline, HLT and L1 level compared to truth with Gaussian fits.

What is previously assumed is confirmed: L1 jets have a significantly lower p_T than jets at other levels. The ratio distributions show the main problem: while the offline and HLT jets have, as ideal, similar transverse momenta as the matching jets at truth level, L1 jets have significantly too low transverse momenta. Not only is the distribution too low, but the resolution - the relative width of the ratio distribution compared to its mean - is also lower than for offline and HLT jets. Because of the too low transverse momentum, it can be expected that the dijet invariant mass of L1 jets is also too low, while those of offline and HLT jets come close to the actual dijet invariant mass. That this is indeed the case can be seen in fig. 3.7.

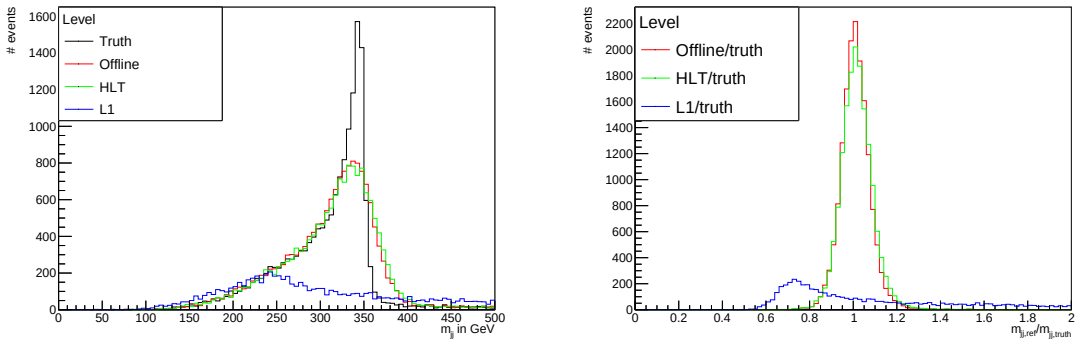

(a) Absolute values (b) Ratios

Fig. 3.7 The m_{jj} distribution is plotted at truth, offline, HLT, and L1 level with p_T cuts of 36 GeV (at L1 level) and 60 GeV (at all other levels). In (a), the absolute distributions of the dijet invariant masses are plotted. In (b), the ratios of the jets at offline, HLT, and L1 level to the respectively matching jets at truth level are plotted.

For calculating the invariant mass, a transverse momentum cut is applied. The transverse momentum cut is 36 GeV for jets at L1 level and 60 GeV for jets at all other levels. The cut is made to ensure that only jets from the event in which the mediator decays to two quarks are considered and not from other events, such as pile-up. For $p_T > 60\,\text{GeV}$, these other events become negligible. Since the L1 jets show a too low p_T, a lower cut is applied. The reasoning behind the lower cut for L1 jets becomes more plausible when the calibration of these jets is introduced in sec. 3.3.

It is insightful to look at how different conditions affect the number of jets in the events. Fig. 3.8 shows that without any cuts or other conditions applied, most events have at least two, but mainly more jets. Especially at truth, offline, and HLT level, many events have a high number of jets. A transverse momentum cut applied at 36 GeV for L1 and at 60 GeV for all other levels, reduces the number of events so that most events at all levels now contain two jets. If only jets that have got a matching jet at truth level are considered, no major change of the distribution is observed. This shows that for higher transverse momenta, jets tend to match to truth level. A jet with higher p_T is more likely to come from the mediator decay, which means that pile-up is negligible for these momenta; this is discussed in sec. 3.1. These jets also appear at truth level and thus have matching jets at truth level. This is not necessarily the case for jets which do not come from these events, for example not for many jets with lower p_T; they do not come from the mediator decay, but rather from pile-up. Hence, they often do not have matching truth jets.

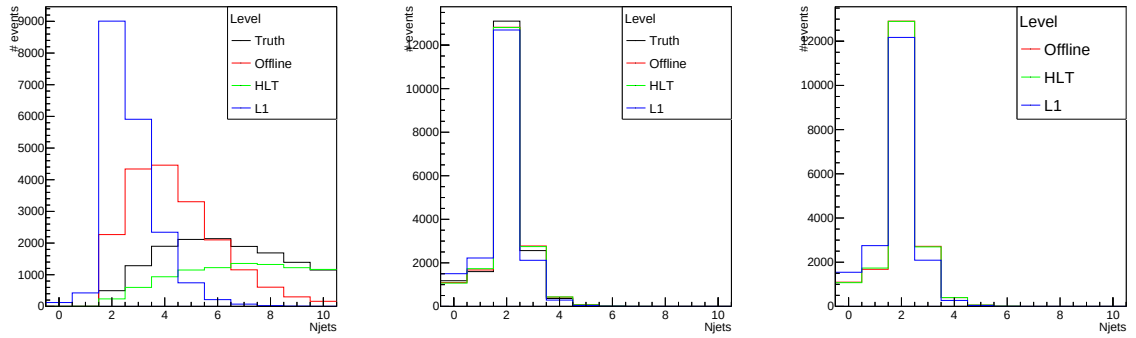

(a) No cut applied (b) With cut applied (c) With cut and matching

Fig. 3.8 Histogram of the number of jets (Njets) in the events when no cut is applied (a), when a p_T cut of 36 GeV (L1 jets), resp. 60 GeV (all other jets) is applied (b), and when the cut and the condition that the jets must have matching jets at truth level are applied (c).

3.3 Calibration of L1 Jets

As seen in fig. 3.7, the dijet invariant mass at L1 level is too low compared with the other levels. This is due to a too low transverse momentum of the L1 jets. The idea is to calibrate the transverse momenta of the L1 jets so that the dijet invariant mass gets closer to truth. Just shifting the p_T, however, would not increase the resolution. The invariant mass peak of the L1 jets was not only too low, but also very broad. In order to increase the resolution, the jets are calibrated dependent on their transverse momentum and their pseudorapidity. For this, the jets are sorted into bins of p_T and η of the L1 jets and the means of the ratios to truth are subsequently derived. It is intuitive that the calibration dependent on the p_T will improve the p_T resolution as it is expected that low-p_T L1 jets deviate more from the truth distribution than high-p_T L1 jets. Through the calibration in η bins, the direction of the L1 jets can be taken into consideration. For jets in the same p_T bin, jets with a higher η will have a higher energy than those with lower η, and thus need a different calibration; it is the energy that is measured by the detector. Furthermore, the detector has variations in η and hence measures different values for jets with same energies when they hit different regions of the detector; these variations would otherwise

be neglected. The bins are chosen to be

$$p_T[\text{GeV}] = [20,\ 60,\ 130,\ 200,\ \infty]$$
$$|\eta| = [0,\ 0.7,\ 1.0,\ 1.3,\ 2.5,\ \infty]\,.$$

The ratios to truth are fitted using a Gaussian distribution (eq. 3.1)

$$f(x) = \frac{A}{\sigma\sqrt{2\pi}} e^{-(\frac{x-\mu}{\sigma})^2} \tag{3.1}$$

with the mean μ, the standard deviation σ, and overall normalisation A. The Gaussian is fitted roughly over the interval in which $f(x)$ is more than a fourth of the peak height to avoid bias from the non-Gaussian tail in further outwards lying regions. An example for a fit can be seen in the appendix in sec. A.1.1. The responses (means) and resolutions (widths) of the fits in the p_T-$|\eta|$ bins are displayed in 3.9.

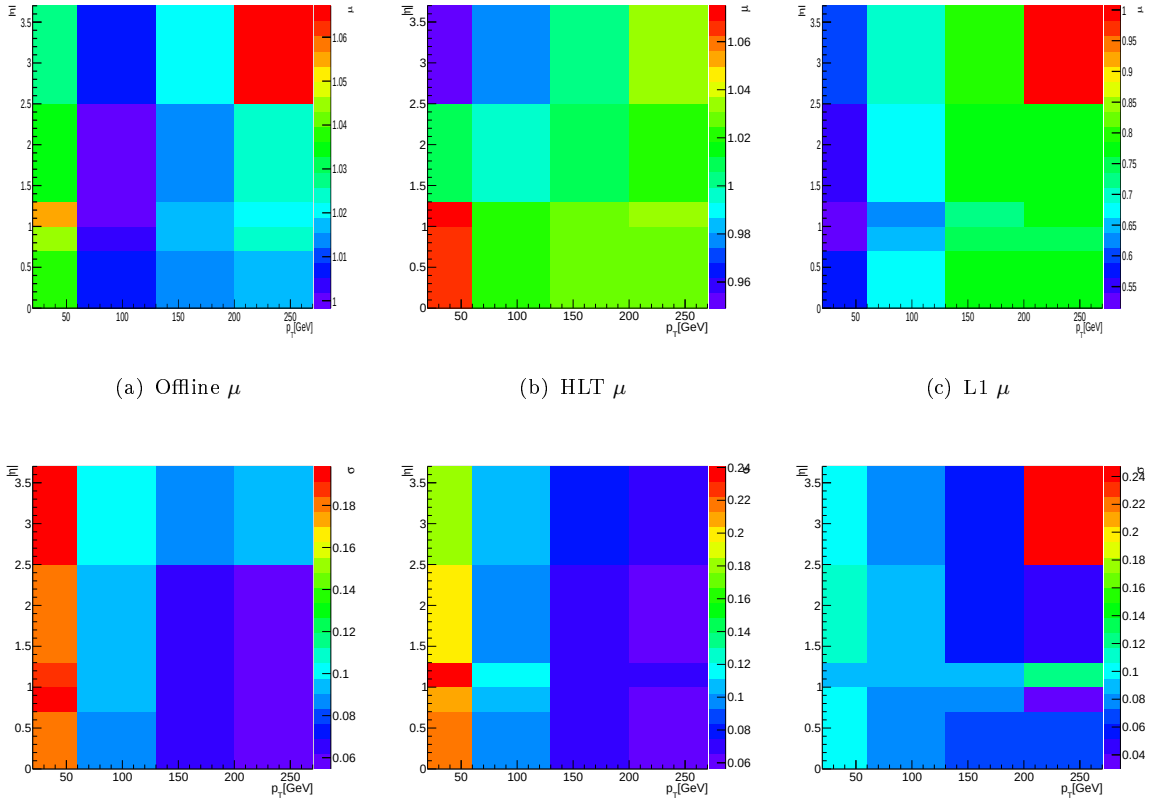

(a) Offline μ (b) HLT μ (c) L1 μ

(d) Offline σ (e) HLT σ (f) L1 σ

Fig. 3.9 The means μ and standard deviations σ for the transverse momentum ratios of jets at offline, HLT and L1 level to jets at truth level for different bins of p_T and $|\eta|$.

One thing that is apparent is that the resolutions are much lower in the region 20GeV $< p_T <$ 60GeV than in the region $p_T >$ 60GeV. The reason for this has been addressed several times: in the lower-p_T region, pile-up is more frequent than in higher-p_T region. This justifies again to apply a p_T cut.

The responses - the values of which can be found in the appendix in sec. A.1.2 - are subsequently used to calibrate the L1 jets. Only to these jets, calibration is applied - the HLT and offline jets are not altered in the following. The calibration is performed by dividing the transverse momenta of all the jets by the response in the p_T-$|\eta|$ bin in which they are. Doing this, the shift of the p_T of the leading and subleading jets at L1 level in comparison to those at HLT level can be seen in fig. 3.10. HLT jets are also shown, because these are the jets that can actually be seen, unlike truth jets.

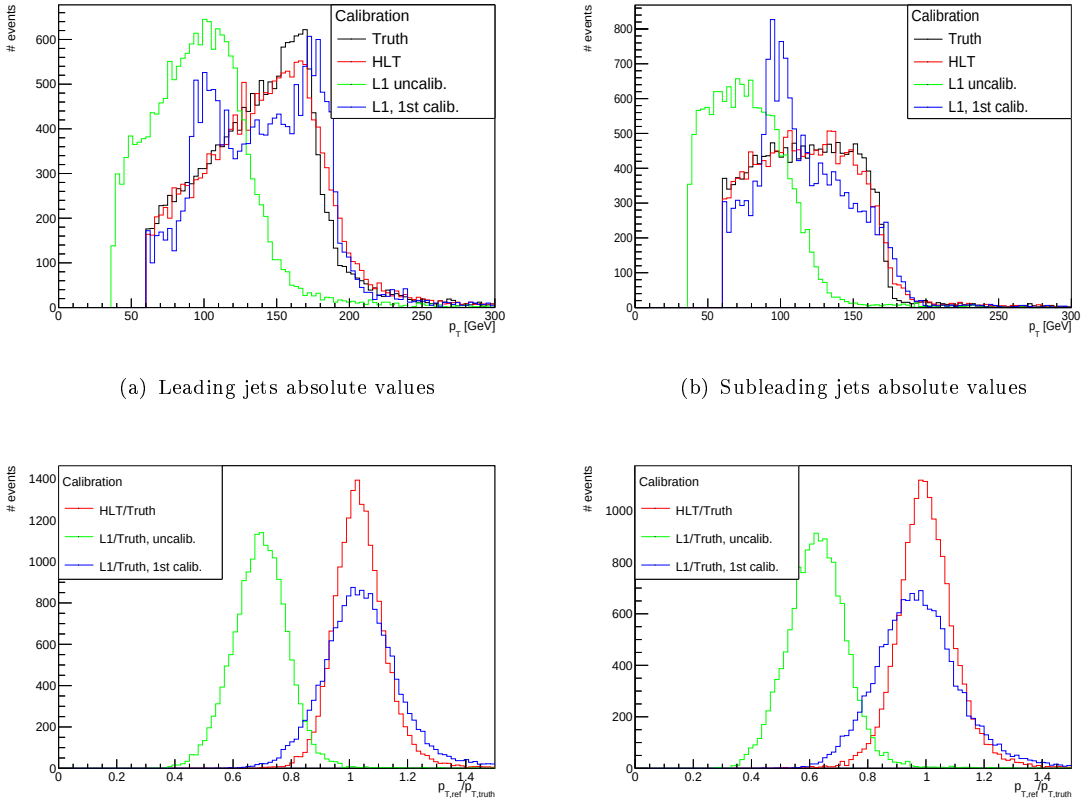

(a) Leading jets absolute values

(b) Subleading jets absolute values

(c) Leading jets ratio

(d) Subleading jets ratio

Fig. 3.10 First calibration of the transverse momenta of the leading (a) and subleading jets (b) at L1 level compared to those at HLT and truth level. In (c) and (d), the ratios to the matching truth level jets are plotted. A cut of $p_T = 36$ GeV for the uncalibrated L1 jets and of $p_T = 60$GeV for the HLT and calibrated L1 jets is applied.

The transverse momenta are indeed shifted in the right direction and are now closer to those of the HLT jets. However, the calibration shifted the shape of the distribution. For the leading jets, the distribution appears to get two peaks. The next step to take is thus to improve the p_T-$|\eta|$ binning and take the features of the transverse momentum distribution of the L1 jets as seen in fig. 3.5 - especially of the leading and subleading jets - more into consideration. Since the distribution is lower than those of the other level, it makes sense to take lower p_T values. Also, in the region of the peak of the leading jets' and subleading jets' p_T distribution, increasing the number of bins is reasonable. Together with an improved $|\eta|$ binning, the p_T-$|\eta|$ binning for the second calibration looks as follows:

$$p_T[\text{GeV}] = [12,\ 36,\ 60,\ 85,\ 100,\ 120,\ 150,\ \infty]$$
$$|\eta| = [0,\ 0.7,\ 1.0,\ 1.3,\ 1.7,\ 2.5,\ \infty]$$

The same procedure is performed as before. The responses are then shown in fig. 3.11.

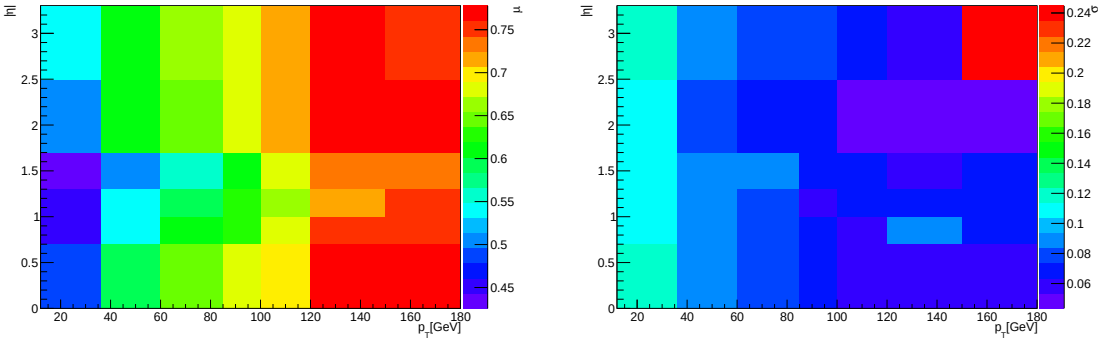

(a) L1 μ (b) L1 σ

Fig. 3.11 The means and standard deviations for the transverse momentum ratios of jets at L1 level to jets at truth level for different bins of transverse momentum and pseudorapidity.

As in the first calibration, the peaks in the low-p_T region are broader and lower than those in the high p_T region. The more detailed binning shows that this, however, is mainly valid for the 12GeV $< p_T <$ 36GeV bin. The responses are again used to calibrate the L1 jets' p_T. Again, the responses are listed in the appendix in sec. A.1.2. The calibration of the transverse momentum is plotted in fig. 3.12, together with the first calibration to better compare those two.

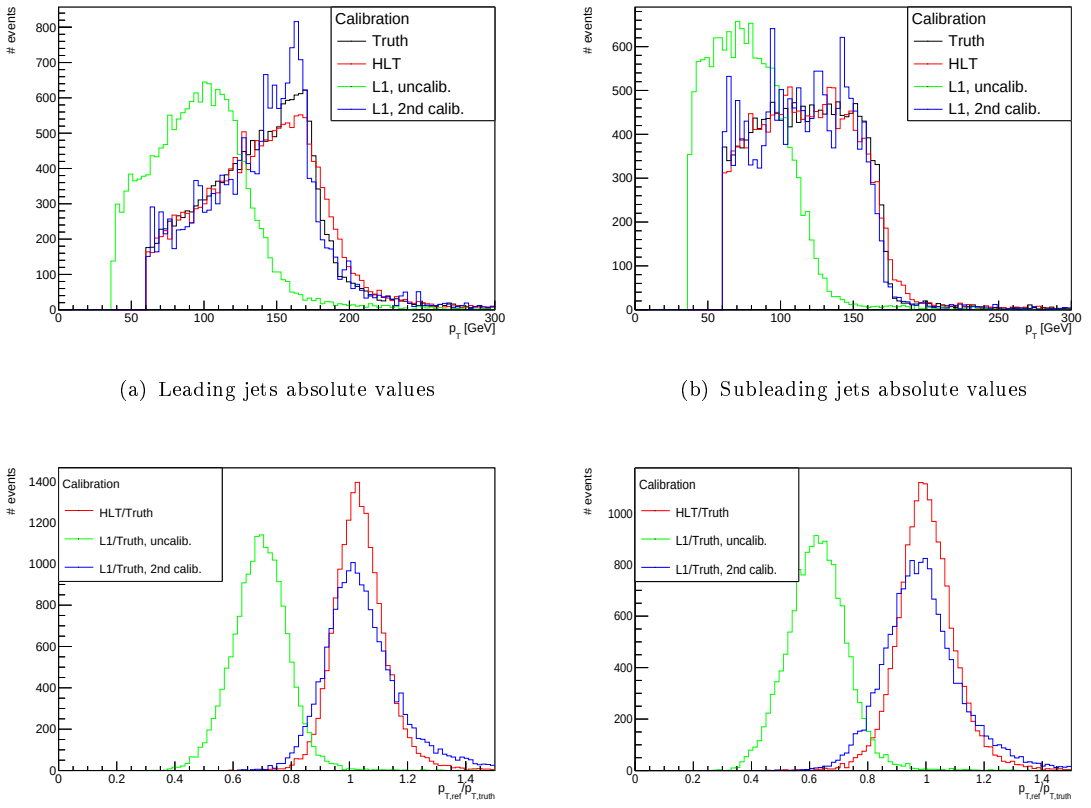

(a) Leading jets absolute values

(b) Subleading jets absolute values

(c) Leading jets ratio

(d) Subleading jets ratio

Fig. 3.12 Second calibration of the transverse momenta of the leading (a) and subleading jets (b) at L1 level compared to those at HLT and truth level. In (b) and (c), the ratios to the matching truth level jets are plotted. A cut of $p_T = 36\,\text{GeV}$ for the uncalibrated L1 jets and of $p_T = 60\text{GeV}$ for the HLT and calibrated L1 jets is applied.

The transverse momentum distribution of the L1 jets look better this time and closer to the transverse momentum distribution of the HLT jets. The two peaks in the leading jets' distribution have shifted closer to each other and now appear closer to the peak of the HLT leading jets' distribution peak. The ratio plots underline this, as the p_T distributions of the calibrated L1 jets are now narrower peaked than after the first calibration. Having calibrated the transverse momenta, the invariant mass of these calibrated jets can now be calculated. The dijet invariant mass distribution can then be seen in fig. 3.13.

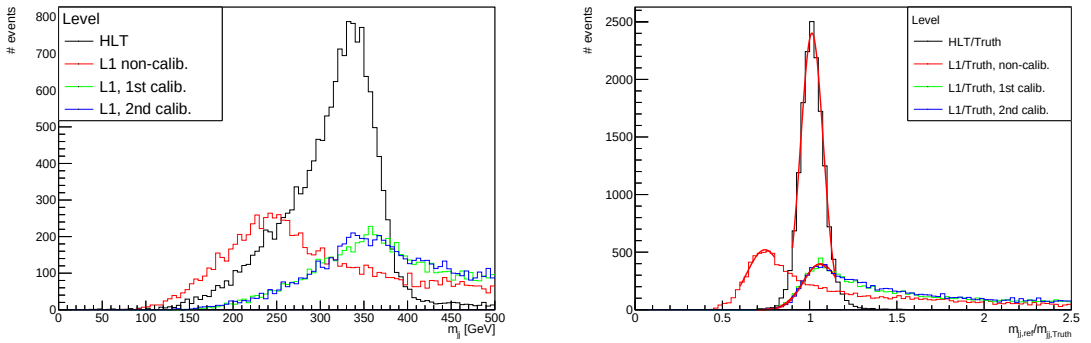

(a) Leading jets (b) Subleading jets

Fig. 3.13 The dijet invariant mass distribution of the uncalibrated L1 jets, the calibrated L1 jets after the first and second calibration in comparison to the dijet invariant mass distribution of the HLT jets.

The means and standard deviations of the L1 to truth dijet invariant mass ratio can be seen in tab. 3.1.

Tab. 3.1 Means and widths of dijet invariant mass ratios of L1 jets to truth jets, before calibration, after first calibration, and after second calibration. Means and widths are extracted from the Gaussian fits.

	μ	σ	μ/σ
L1, uncalibrated	0.74±0.01	0.11±0.01	0.14±0.01
L1, 1st calibration	1.1±0.1	0.10±0.01	0.096±0.002
L1, 2nd calibration	1.1±0.1	0.094±0.003	0.089±0.003

It can be seen that the calibrations indeed shift the means to 1. Also, the resolutions can be improved as the widths of the ratios are lower for the calibrated jets than for the uncalibrated jets. The second calibration is a further improvement to the first calibration.

Chapter 4

Outlook

4.1 Conclusion

Based on the studies that are conducted it this thesis, it can be concluded that a calibration of the L1 jets based upon the responses of the transverse momentum in bins of the transverse momentum and the pseudorapidity yields certain improvements. It shifts the transverse momentum, which is now much closer to truth level. Using the calibrated transverse momentum, the dijet invariant mass can be shifted closer to the real value and the resolution can be improved, from 14% to 8.9%. A finer binning in transverse momentum can further improve the calibration, as can be seen when comparing the second calibration to the first calibration. As the responses are mainly dependent on the transverse momentum, rather than on the pseudorapidity, a finer binning of the transverse momentum will be more useful than one of the pseudorapidity. The improvements by doing this, however, will be limited; there is a more visible improvement in the distributions of the transverse momentum than there is in the distribution of the dijet invariant mass. More than only the responses should be used. Calibrating the L1 jets by calibrating their transverse momenta in dependence of the transverse momentum itself and the pseudorapidity can thus be a first step. Further detector effects should, however, be taken into consideration to improve the calibration and allow the L1 jets to be better used for further analysis.

4.2 Future studies

The studies show to which extent the calibration of the transverse momenta of the L1 jets yield a calibration of their dijet invariant mass. The calibration of the L1 jets' transverse momenta using their responses in bins of p_T and $|\eta|$ yields an improvement of the resolution, both of the transverse momentum and the dijet invariant mass distribution. It also shifts the distributions closer to truth level. It is shown that a finer binning, especially in p_T, further improves the calibration. However, the thesis could also show that the improvements coming from this calibration of the transverse momentum with limited information available only has a limited influence on the dijet invariant mass. The low amount of information comes as a result of the current detector, and more complicated effects cannot be studied in the extent that they should be. If more detailed calorimeter information were available at L1, the calibration could be improved. This will be possible in the future, when the readout and trigger system will have been updated. Then, the fraction of energy in each of the calorimeter layer will be known, which can subsequently be used for a better calibration of the jets. These are all things that can be studied further.

The calibration of the L1 jets is necessary to pursue the idea of a new Dark Matter search that makes use of these jets. It would help to examine the possible existence of a new mediator between Dark Matter and Standard Model particles. The successful outcome of the search is dependent of the quality of the calibration of the L1 jets. The calibration that was applied in this thesis involved reasonable improvement, but not to that extent as it, desirably, would be. Further studies are advisable and worthwhile, especially with an improved L1 system. In conclusion, the L1 jets calibration can be a valuable step in optimising the search for Dark Matter, one of the big mysteries of modern physics and one of the most important research focusses of current particle physics.

Appendix A

Appendix A

A.1 Calibration

A.1.1 Fitting the ratios

As described in sec. 3.3, the responses are derived by fitting the ratios with a Gaussian function. It is fitted over a range in which the values are more than a fourth of the peak height. This is done to avoid the non-Gaussian tail of the distribution. It is not important that this is done meticulously, as long as the distribution follows a Gaussian distribution in the range. An example, in this case for the $60 < p_T[\text{GeV}] < 130$ and $0.7 < |\eta| < 1.0$ bin is seen in fig. A.1.

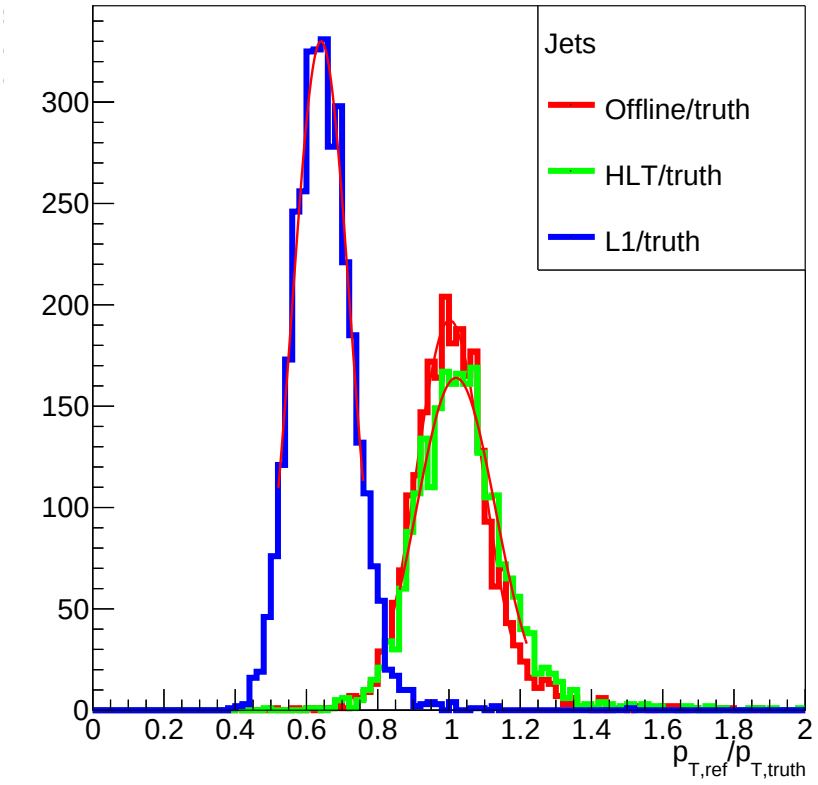

Fig. A.1 Example of the fitting of the ratio in the bin $60 < p_T[\text{GeV}] < 130$ and $0.7 < |\eta| < 1.0$. On the y-axis, the number of events are plotted.

A.1.2 Tables of responses

The responses of the L1-to-truth transverse momentum ratios that are used for the first calibration are listed in tab. A.1.

Tab. A.1 Responses of the L1-to-truth transverse momentum ratios used for the first calibration. Unless stated otherwise, the error is 0.01.

p_T[GeV] \ $\lvert\eta\rvert$	[0, 0.7]	[0.7, 1.0]	[1.0, 1.3]	[1.3, 2.5]	[2.5, ∞]
[20, 60]	0.57	0.52	0.51	0.54	0.59
[60, 130]	0.68	0.64	0.63	0.67	0.69
[130, 200]	0.78	0.75	0.72	0.77	0.79
[200, ∞]	0.78	0.74	0.76±0.06	0.78	1.0±5.1

The large error in the $p_T > 200\,\text{GeV}$, $|\eta| > 2.5$ bin is due to the fact that only a very small number of jets fall into this bin so that it is very hard to fit those. Since only a small number of jets are affected by this, this has a very limited influence on the overall calibration and thus is negligible.
The responses used for the second calibration are listed in A.2.

Tab. A.2 Responses of the L1-to-truth transverse momentum ratios used for the second calibration. The error is 0.01.

p_T[GeV] \ $\lvert\eta\rvert$	[0, 0.7]	[0.7, 1.0]	[1.0, 1.3]	[1.3, 1.7]	[1.7, 2.5]	[2.5, ∞]
[12, 36]	0.49	0.45	0.45	0.43	0.50	0.53
[36, 60]	0.59	0.55	0.54	0.50	0.61	0.62
[60, 85]	0.65	0.60	0.59	0.56	0.65	0.66
[85, 100]	0.67	0.63	0.62	0.61	0.69	0.68
[100, 120]	0.70	0.68	0.67	0.68	0.71	0.71
[120, 150]	0.76	0.75	0.72	0.74	0.76	0.77
[150, ∞]	0.77	0.74	0.74	0.73	0.78	0.75

References

[1] Katherine Garrett and Gintaras Duda. Dark matter: A primer. Adv. Astron., 2011:968283, 2011.

[2] Michael Barnett and Erez Etzion. A search for new physics processes using dijet events. http://atlas.cern/updates/atlas-news/search-new-physics-processes-using-dijet-events, Jun 2011. Accessed: 2017-04-17.

[3] Search for light dijet resonances with the ATLAS detector using a Trigger-Level Analysis in LHC pp collisions at $\sqrt{s} = 13$ TeV. Technical Report ATLAS-CONF-2016-030, CERN, Geneva, Jun 2016.

[4] Planck and the cosmic microwave background. http://www.esa.int/Our_Activities/Space_Science/Planck/Planck_and_the_cosmic_microwave_background, 2017.

[5] Wayne Hu and Martin White. The cosmic symphony. Scientific American, 290:44–53, Feb 2004.

[6] Brian R Martin and Graham Shaw. Particle Physics. Manchester Physics Series. Wiley, 2008.

[7] Leif Jönsson. Lectures in particle physics, 2016.

[8] Cheuk-Yin Wong. Introduction to High-energy Heavy-ion Collisions. World Scientific, 1994.

[9] About the ATLAS experiment. https://atlas.cern/discover/about, 2017. Accessed: 2017-03-12.

[10] Detector & technology. https://atlas.cern/discover/detector, 2017. Accessed: 2017-03-12.

[11] Calorimeter. https://atlas.cern/discover/detector/calorimeter, 2017. Accessed: 2017-03-12.

[12] Michel Goossens. Calorimetry. http://atlas.web.cern.ch/Atlas/TP/NEW/HTML/tp9new/node9.html#SECTION00432000000000000000, Jan 1995. Accessed: 2017-03-12.

[13] Lucas Taylor. Muon detectors. http://cms.web.cern.ch/news/muon-detectors, Nov 2011. Accessed: 2017-03-12.

[14] PyROOT | ROOT a data analysis framework. http://root.cern.ch/pyroot, Mar 2017. Accessed: 2017-03-22.

[15] ROOT a data analysis framework | ROOT a data analysis framework. http://root.cern.ch, Mar 2017. Accessed: 2017-03-22.

[16] Zachary Marshall and the Atlas Collaboration. Simulation of pile-up in the ATLAS experiment. Journal of Physics: Conference Series, 513(2):022024, 2014.